Study on methods to extract high contrast image in active dynamic thermography

Saxena, Ashish; Raman, Vignesh; Ng, Eddie Yin Kwee

2019

Saxena, A., Raman, V., & Ng, E. Y. K. (2019). Study on methods to extract high contrast image in active dynamic thermography. Quantitative InfraRed Thermography Journal, 16(3-4), 243-259. doi:10.1080/17686733.2019.1586376

https://hdl.handle.net/10356/144497

https://doi.org/10.1080/17686733.2019.1586376

Study on Methods to Extract High Contrast Image in Active Dynamic Thermography

Ashish Saxena*, Vignesh Raman, EYK Ng

School of Mechanical and Aerospace Engineering, Nanyang Technological University, 50 Nanyang Ave, Singapore, 639798

*Corresponding Author: ashish008@e.ntu.edu.sg

Abstract

In the present study, image reconstruction methods are applied in active dynamic thermography (ADT) to visualize the superficial blood vessel with high contrast. ADT is performed on the left forearm of a human subject by applying cooling based external thermal stimulation. Both non-parametrized, viz. sequence image, sequentially subtracted image, Discrete Fourier Transformation (phase and amplitude image), and Thermographic Signal Reconstruction (TSR), and parametrized, viz. Tau time ($\boldsymbol{\tau}$), dT_{norm}, t_{90-10n}, and Tissue Activity Ratio (TAR), types of image reconstruction methods are used. To perform a quantitative comparison, among the image reconstruction methods, the image contrast value is evaluated. While sequentially subtracted image provides a high contrast image in non-parametrized image reconstruction methods, for parametrized image reconstruction methods, it is TAR. Among all the methods considered, TAR provides the best contrast image followed by $\boldsymbol{\tau}$ image method.

Keywords: Active Dynamic Thermography; Thermal Image Reconstruction; Image Contrast; Tissue Activity Ratio; Tau time.

1. Introduction

Active dynamic thermography (ADT), wherein transient sequence of images result upon application of an external thermal or pressure excitation, is one of the most useful quantitative thermography methods in medical diagnosis [1]. Since a diseased tissue responds differently to the external excitation as compared to a normal tissue, ADT proves to be an efficient tool in diagnosing various diseases, such as breast tumor detection, Raynaud's disease, burn wounds, etc. [2]–[4]. While external excitation improves the image contrast that eases the target feature extraction, it also leads to the generation of a large amount of sequence image data to be analyzed. Moreover, the contrast of the image sequence decreases as the recovery phase progresses upon removal of the excitation source [5]. Therefore, reconstruction of a single synthetic image, which is both qualitatively and quantitatively advanced (feature contrast and diagnosis parameter) as compared to the whole image sequence, is needed. To do so, application of various image reconstruction algorithms, to ADT problems, is summarized hereafter.

It is well known that the original sequence images have a lower signal to noise ratio (SNR). SNR can be improved by deriving phase and amplitude images using Fourier transformation (FT) [6], [7]. In such an attempt, Boue et al. [8] evaluated the diameter of the superficial vein using thermographic amplitude images, of which the contrast is found to be comparatively better than the transient sequence images. Using fast Fourier transform (FFT), Liu et al. [9] showed that the large sub-cutaneous veins can be distinguished from microvasculature and skin tissue without the blood vessel, respectively, in the frequency range of 0.005 to 0.06 Hz. Given that an adequate contrast enhancement cannot be achieved in all the patients, application of thermographic signal

reconstruction (TSR) method, which is conventionally used in the field of material characterization and defect detection by ADT [10]–[13], is shown in the work of Liu et al. [14]. The authors have applied a 5-minute cuff-based occlusion, followed by transient thermal image acquisition during the reactive hyperaemia. At each pixel, the coefficient values are derived from the first derivative of the logarithmic equation fit to the temperature response over time, and a synthetic image is reconstructed. The authors have shown a substantial improvement in SNR that helps in clear visualization of the angioarchitecture in the synthetic image.

Since ADT involves a transient process of recovery to normal state post external excitation, to reconstruct the synthetic image, pixel specific parameters pertaining to thermal recovery can also be extracted. One such parameter is the thermal time constant (called Tau time, '$\boldsymbol{\tau}$') that quantifies the thermal activity of the tissue. Given the apparent difference in heat transfer rate between the skin tissue with and without vein, it is imperative that the $\boldsymbol{\tau}$ time evaluation would differentiate the two; hence, brings out the contrast in the resultant $\boldsymbol{\tau}$ image. This image can be used to diagnose skin tissue with pathological conditions as described in the work of Foerster et al. [15], wherein the authors have developed a $\boldsymbol{\tau}$ image based tool to diagnose Raynaud's phenomenon (RP). Further, to estimate the $\boldsymbol{\tau}$ value more accurately, a non-linear regression-based exponential curve fitting to the experimental data can be done. This method is applied to monitor the cardiosurgery [16]–[18], evaluation of burn wound healing [19]–[21], vascular disease diagnosis [22], etc. Recently, Moderhak et al. [23] described a dynamic thermography method, wherein 60 seconds of thermal excitation and 180 seconds of recovery time is used, to quantitively determine the success of breast reconstruction procedure by skin flap perfusion assessment. The authors have used a Simplified Magnitude-Temporal Parametrization method

(SMTP) to define two unique parameters: dT_{norm} and t_{90-10n} [24], at each pixel, to reconstruct a single image from the ADT sequence, respectively. With the help of the improved contrast images, reconstructed using these two parameters, the authors have shown that the two groups of patients, who will either develop post-surgery necrosis complications or not, can be diagnosed at an early stage. In our recent work [25], a novel method of single image reconstruction, TAR image, is introduced. Comparing the new method with the existing $\boldsymbol{\tau}$ image method, in three subjects, it is reported that the TAR image provides a quantitative and qualitative high contrast image.

It is evident from the literature review that there exist many single image reconstruction methods that can be applied to the ADT sequence. The reconstructed single thermal image is useful for both qualitative and quantitative analysis of the tissue health monitoring. However, a comprehensive comparison of various image reconstruction methods, applied to a single ADT problem, is not found in the literature. Therefore, in the present study, with the application of cooling excitation, ADT sequence is captured, on the forearm of a human subject, to visualize the superficial vein with high contrast. To do so, various pre-existing image reconstruction methods, viz. FT image (amplitude and phase), TSR image, and parametric image ($\boldsymbol{\tau}$, dT_{norm}, t_{90-10n}, $and\ TAR$), are used, and a comparative study is done. A contrast factor (W), to quantitatively compare the images obtained from each of the image reconstruction methods studied, is introduced.

2. Method and Material

2.1. Experiment Setup and Procedure

In-vivo human subject tests are carried out on 3 male subjects (age: 24 ± 1 years), under an approved ethical study, at Nanyang Technological University, Singapore (IRB: SHS-NTU/014/2016). In this experiment, a continuous cooling is applied on the left forearm of each subject for 30 seconds. The cooling application is done with the help of a cooling pad [26] recirculated with ice water at a temperature of 5 ± 0.5 ºC. After the removal of cooling, 90 seconds of sequential thermal images are captured by an Infrared (IR) thermal camera (VarioCam by InfraTec) at a rate of 2 frames per second (Figure 1). Experiments are performed after allowing the subject to sit for 15 minutes in a controlled temperature environment of 22 ± 0.5 ºC. In each subject, the average value of temperature with standard deviation (± SD), over the skin tissue (within the cooling stimulation zone) at the start of the experiment, after the removal of cooling, and end of rewarming, is summarized in Table 1.

2.2. Non-parametric image reconstruction methods

2.2.1. Discrete Fourier Transformation

For the ADT experiment performed in the present study, Figure 2 shows the variation of skin temperature (T_{skin} in ºC) normalized by core body temperature (T_{core} = 37 ºC) versus time (s). On the removal of the external excitation, to transform the resultant time domain temperature progression into frequency domain, at each pixel within the cooling zone, 1-Dimensional (1-D) Discrete Fourier Transform (DFT) can be applied. The equation for 1-D DFT is given below [7]:

$$F_n = \Delta t \sum_{k=0}^{N-1} T(k\Delta t) e^{\frac{-j2\pi nk}{N}} = Re_n + Im_n \quad (1)$$

Where, n designates the frequency increment (n=0,1, 2, …N), k is the discrete number of temperature (T in ºC) samples, Re_n and Im_n represents the real and imaginary parts of the transform, respectively, at given n, j is the imaginary number, and Δt represents the time interval (s). Using the result of Eq. (1), the modulus or amplitude (A in ºC) and phase delay (φ in rad) is computed using the following formulae:

$$A = \sqrt{Re_n^2 + Im_n^2} \tag{2}$$

$$\varphi = arctan\left(\frac{Im_n}{Re_n}\right) \tag{3}$$

Application of DFT, to the temperature profile obtained after the removal of cooling excitation, results into a Hermite function [27]. A Hermite function has a symmetrical real and an asymmetrical imaginary part (at N/2). Since both the first and second half of the frequency range (around 0 Hz) produce alike results, only N/2 useful frequencies are considered for further analysis. For the retained N/2 frequencies, the corresponding phase and amplitude images are extracted.

2.2.2. Thermographic Signal Reconstruction (TSR)

In this method, a logarithmic polynomial function of degree m (Equation 4) is fit to the log of temperature versus time plot, at each pixel, after the removal of cooling.

$$\log_{10}(dT) = a_0 + a_1 \log_{10}(t) + a_2[\log_{10}(t)]^2 + \ldots + a_m[\log_{10}(t)]^m \tag{4}$$

where, dT is the temperature (ºC) increase as a function of time, t (s). a_m is the coefficient of the polynomial function of degree m. The polynomial function is chosen such that the transient series of images can be reduced to $(m + 1)$ number of images. The choice of polynomial degree m is conventionally done with the help of an optimization method, wherein images

corresponding to the range of m and its respective coefficient ranks are compared to select the best contrast image revealing maximum thermal expressions [12]. Using this chosen polynomial degree, first derivative images are extracted for further analysis.

2.3. Parametric Image Reconstruction methods

2.3.1. Tau Image:

The natural rewarming of the skin tissue, to the cooling excitation, can be analyzed using lump capacity analysis model, wherein a uniform rewarming is assumed under the influence of ambient convention thermal boundary condition [28]. This process can be characterized with the help of thermal time constant (called Tau time, '$\boldsymbol{\tau}$') which is equal to the time required for a system response to decay to zero [29]. Further, as shown in the work of Dupuis [4], Foerster et al. [15], Jankovic et al. [22], Meffert et al. [30], Merla et al. [31], etc., the rewarming process closely resembles to an exponential response curve described by the transient first order response as given by Equation 5.

$$T(t) = T_o + \Delta T(1 - e^{-t/\tau}) \quad (5)$$

where, $T(t)$ is the temperature (°C) at any time instant, t (s), T_o is the initial temperature (°C), ΔT is the total temperature change (°C), and $\boldsymbol{\tau}$ is the Tau time (s). When the rewarming process reaches the $\boldsymbol{\tau}$ time, the temperature of the system attains $\left(1 - {}^{1}/_{e}\right)$ times of total temperature difference between the initial and post excitation temperature (dT_{excite} in °C), which is equal to 63% of dT_{excite}. At each pixel, Tau time ($\boldsymbol{\tau}$) is calculated (Figure 2), followed by replacing the original sequence image pixel value with the evaluated $\boldsymbol{\tau}$ value, and thereby, a $\boldsymbol{\tau}$ image is reconstructed. This $\boldsymbol{\tau}$ image is an equivalent representation of the whole thermal image sequence.

2.3.2. dT_{norm} and t_{90-10n} Image:

As defined in the work of Moderhak et al. [23], dT_{norm} and t_{90-10n} is calculated as follows:

$$dT_{norm} = \frac{dT_{recovery}}{dT_{excite}} \quad (6)$$

$$t_{90-10n} = \frac{t_{90-10}}{t_{recovery}} \quad (7)$$

where, $dT_{recovery}$ is the temperature difference (°C) between the start and end of the allowed experimental thermal recovery, dT_{excite} is the temperature difference (°C) between the start and end of the thermal excitation, t_{90-10} is the difference in time (s) to reach 90% and 10% of the $dT_{recovery}$, respectively, ($t_{90-10} = t_{90\%\ of\ recovery} - t_{10\%\ of\ recovery}$), and $t_{recovery}$ is the total experimental time (s) of the thermal recovery (Figure 2).

2.3.3. Tissue Activity Ratio (TAR) Image

In this method, a novel approach to reconstruct a unique image, based on the individual pixel's thermal activity, is used [25]. On removal of the external cooling, it is evident that pixel just above the blood vessel would show a higher thermal activity as compared to the other pixels; hence forms the basis for a qualitatively and quantitatively advanced image. Using Equation 8, the thermal activity during the rewarming phase, at each pixel, can be quantified with the help of a ratio called as Tissue Activity Ratio (TAR). TAR accounts for both the rewarming as well as the excitation phase. First, a reference recovery temperature (T_r in °C), for all the pixels within the excitation zone, is fixed. This is done by finding the maximum value of temperature reached at each pixel during the recovery phase, and then select the minimum of these values. The selected T_r value ensures that all the pixels will reach at least this temperature within the acquired recovery duration (90s in the present study). Using this T_r value, at each pixel, the time

of rewarming (t_r in s), to rewarm from the temperature at the end of cooling (T_c in ºC) to T_r, is evaluated and thus, the rate of rewarming (RR in ºC/s) is calculated (Equation 9). Further, the rate of cooling (RC in ºC/s), at each pixel, is calculated (Equation 10) by subtracting the temperature at the end of the cooling (T_c in ºC) from the initial temperature (T_i in ºC) before application of cooling, and dividing the resultant temperature difference by the total duration of application of cooling (t_c in s). Unlike the value of t_r in the rewarming phase, the time for cooling (t_c) will be same for all the pixels. The mathematical formulation to calculate TAR, at each pixel, within the cooling zone is given below:

$$TAR = \frac{RR}{RC} \tag{8}$$

where, $$RR = \frac{T_r - T_c}{t_r} \tag{9}$$

$$RC = \frac{T_i - T_c}{t_c} \tag{10}$$

Computing TAR value at each pixel, a unique TAR image is reconstructed.

2.4. Image Contrast Analysis

To compare and evaluate the quality of an image, a contrast factor (W) is evaluated. The contrast factor defines the relative strength of an image target parameter with respect to the background. In the present study, the feature of interest (target) is the superficial vein around the skin tissue (background). A high value of W refers to a better visibility of the superficial vein in the image. Using the Weber's formula [32], W is defined as follows:

$$W = \left|\frac{I - I_b}{I_b}\right| \tag{11}$$

where, I and I_b are the image parameter over the skin tissue with (target) and without superficial vein (background), respectively. In the present study, average values of I and I_b are taken from the reference sampling locations (black and red-dashed rectangular boxes) as shown in Figure 3. While I is taken over the superficial vein (target), I_b is taken from the neighboring skin tissue (background). These reference sampling locations, in each subject, are consistently used for all the images extracted from the various image reconstruction methods studied.

In Equation 11, the value of I_b is essentially less than the value of I [32], therefore, the value of W provides a measure of difference in the image parameter, between the two regions (target and background), with respect to the minimum of the image parameter over the two regions. By default, it is considered that the background will have the minimum image parameter value as compared to the target ($I > I_b$), however, this is not true in all the cases. For comparison purpose, if all the images, resulting from different image reconstruction methods, provide a trend of either $I > I_b$ or $I < I_b$ consistently, the resultant contrast comparison is balanced. However, if any of the images deviate from the adopted consistent trend, the resultant contrast comparison is imbalanced. In the present study as well, $I > I_b$ is adopted as a consistent trend. To perform a balanced comparison, irrespective of $I > I_b$ or $I < I_b$ trend in the images, the Weber's formula (Equation 11) should be modified (W') such that the minimum of I or I_b should be used in the denominator (as given by Equation 12).

$$W' = \left|\frac{I - I_b}{\min(I,\ I_b)}\right| \tag{12}$$

On the other hand, to maintain the standardized usage of the Weber's contrast formula (Equation 11) and present a balanced comparison among the adopted ($I > I_b$) and deviating ($I < I_b$) trend

images, the deviating trend images can be transformed using the following inversion formulation:

$$\emptyset'_{ij} = \left(\frac{1}{\emptyset_{ij}}\right) * \emptyset_{ij_{max}} \quad (13)$$

where, i and j are the number of row and column, respectively, to locate the target pixel, $\emptyset'_{ij}$ and $\emptyset_{ij}$ are the transformed and original image parameter, respectively, and $\emptyset_{ij_{max}}$ is the maximum image parameter value of all the pixels in the original image. Using Equation 13, the value of I and I_b (where, $I < I_b$) can be transformed as follows:

$$I' = \left(\frac{1}{I}\right) * \emptyset_{ij_{max}} \quad (14)$$

$$I'_b = \left(\frac{1}{I_b}\right) * \emptyset_{ij_{max}} \quad (15)$$

The proposed transformation results into an equivalent image as the original image but with an inverted scale (inverse proportionality), which provides the desired $I' > I'_b$ trend. Given the multiplication with $\emptyset_{ij_{max}}$ in Equation 14 and 15, the resultant I' and I'_b are dimensionless in nature. Using the standard Weber's contrast formula (Equation 11), the contrast for the transformed image (with I' and $I_b{}'$) can be calculated as follows:

$$W = \left|\frac{I - I'_b}{I_{b'}}\right|, \text{ where } I' > I'_b \quad (16)$$

Replacing the value of I' and I'_b from Equations 13 and 14, Equation 15 will result into Equation 17.

$$W = \left|\frac{I_b - I}{\mathrm{I}}\right|, \text{ where } I < I_b \quad (17)$$

Since Equation 17 follows the generic nature defined by the modified Weber's contrast formula in Equation 12 (using minimum of I or I_b in the denominator for a balanced comparison among the adopted ($I > I_b$) and deviating ($I < I_b$) trend images), the contrast calculated from the standard Weber's formula (Equation 11), using a transformed value of I and I_b (where, $I < I_b$), will provide a balanced comparison with the images following the adopted $I > I_b$ trend.

3. Results and Discussion

3.1. Transient sequence images

After the removal of the external stimulation (cooling), before reaching the original thermal equilibrium with the ambient surroundings, the skin tissue undergoes a transient recovery phase. The thermal activity of the skin tissue, due to blood perfusion and blood flow in the superficial vein, determines the rate of the recovery process. It is evident that the skin tissue over the superficial vein will recover faster as compared to the surrounding skin tissue with no such vein. This brings out the contrast in the visibility of the superficial vein. However, the dynamic sequence images do not hold a consistent clear visibility of the blood vessel as the recovery progresses further. Given the rate of recovery is directly proportional to the temperature difference, due to a continuous decrease in the temperature difference, the rate of recovery slows down as the recovery progresses. Therefore, the visibility of the superficial vein with reference to the nearby skin tissue region first increases and then decreases. To quantify this characteristic, using Equation 11, the contrast of the superficial vein, in all the sequence images, is calculated. Plotting the superficial vein contrast, in all subjects, against time, Figure 4 corroborates with the fact that the visibility of the superficial vein changes dynamically throughout the recovery phase.

3.2. Non-parametric image reconstruction

3.2.1. Best contrast image from the sequence

Marking the peak of the contrast curve in Figure 4, the maximum contrast point ($W_{max.}$) is determined, which is in the range of 0.2 to 0.6 in the three subjects studied. Using the $W_{max.}$ point, a single high contrast image, from the transient sequence of images, can be selected. In each subject, Table 2 shows the image corresponding to $W_{max.}$ point. A contrast value of less than 1 suggests a poor visibility of the superficial vein. It is to be noted that the occurrence of $W_{max.}$ point differs in all the subjects. This is because of the different morphological and hemodynamic characteristics, like thickness of the skin tissue, diameter of the superficial vein and its blood flow velocity, skin tissue blood perfusion rate, etc., which bring varied intensity of thermal activity in each subject and hence, either speed-up or delay the occurrence of $W_{max.}$ point. In Subject-2, the $W_{max.}$ point occurs much later ($W_{max.} = 0.21$ at 40 s) as compared to Subject-1 ($W_{max.} = 0.56$ at 22 s) and Subject-3 ($W_{max.} = 0.61$ at 26.5 s).

3.2.2. Sequential image subtraction

To further enhance the contrast of the sequence images, a primitive noise subtraction technique can be used [26], wherein the very first image after the removal of the cooling (external thermal excitation) is subtracted from the subsequent images in the recovery phase. Given the image to be subtracted is always the same, it is imperative that the contrast of all the subsequent images will increase by a same fraction. Hence, in each subject, to evaluate the highest enhancement in the contrast, the subtracted image corresponding to the $W_{max.}$ point in the original sequence images is selected. From Table 2, it can be observed that the qualitative visibility of the superficial vein in the subtracted images, in all subjects, is better than the corresponding original

sequence images. Quantitatively, from Table 5, the contrast of the subtracted images, in all the three subjects, is found to be improved by 52%, 76%, and 28%, respectively, as compared to the corresponding sequence images.

3.2.3. Amplitude and phase image

From the amplitude and phase images, obtained across multiple frequencies through DFT processing, the blind frequency, at which the region of interest (RoI) in the image is clearly visible with high contrast, is determined; RoI corresponds to the superficial vein in the present study. From the literature, it is noticed that there are mainly two methods to find out the blind frequency [27]. In the first method, the phase value over the RoI is plotted against the frequency and the frequency corresponding to the point of inflexion is chosen as the blind frequency. In the second method, the phase contrast between the RoI and the surrounding is plotted against the frequency values, and the frequency corresponding to the maximum contrast value is chosen as the blind frequency. In the present study, the latter method is adopted, wherein using the Weber's contrast formula (Equation 11), the best contrast amplitude and phase images are extracted (Table 2). Given the phase image, for Subject-1 and 2, shows a lower descriptor value over the blood vessel as compared to the background ($I < I_b$), contrast value is calculated after performing the image transformation using Equation 13. For subject-1, 2, and 3, the blind frequencies for phase images are found to be 0.19 Hz, 0.1 Hz, and 0.18 Hz, respectively. Except for Subject-2, the best contrast amplitude images occur at a different frequency than the blind frequency, which is 0.23 Hz and 0.09 Hz for Subject-1 and Subject-3, respectively. From Table 5, it can be observed that the contrast value of amplitude images is always higher than phase images. This can be further corroborated by the visual inspection of the images in Table 2, where the phase images, in all subjects, show more non-uniformity in the background skin tissue

regions as compared to amplitude images; this degrades the visible quality of the target superficial vein. However, the qualitative clarity of superficial vein in the phase images is found to be better than the amplitude images, viz. the visibility of the branching blood vessel in Subject-1 and the diffusion around the superficial vein in Subject-2 and 3.

3.2.4. TSR coefficient image

In the present study, three degrees of polynomial ($m = 4, 5\ and\ 6$) are tested for the best contrast image. Using these polynomial equations, at each pixel, the first derivative is calculated, and the respective coefficient values (a_m) are used to extract m number of images. To select the best image, in each subject, contrast value (W using Equation 11) is calculated, and the coefficient image with highest contrast value is selected. As observed in Table 3, the best contrast image, for both Subject-1 and 2, is found at $m = 4$ and a_4, while for Subject-3, it is found at $m = 5$ and a_1. However, the corresponding images (Table 2) do not comply with the high contrast values in Table 5. This high contrast value is the outcome of the outliner regions in the image; leads to a very low value of the background image parameter (I_b) as compared to the target image parameter (I). This effect is mainly observed in Subject-2 and 3, which results into a qualitatively poor image but with an unrealistically high contrast value.

3.3. Parametric image reconstruction

Reconstruction of a single image, from ADT sequence, not only provides a qualitative representation, but also includes quantitative information. This quantitative information, at each pixel, provides the heat flow characteristics. To do so, quantitative parameters, during the rewarming phase, can be defined. The basis for any of these parameters is the quantification of thermal activity of the tissue, which can be defined as the measure of degree of responsiveness to

the external stimulation. This responsiveness, in terms of heat transfer, is the result of the tissue blood perfusion. In the present study, other than the skin tissue perfusion, presence of a superficial vein, which acts as an additional heat source, leads to a higher responsiveness to the external stimulation as compared to the tissue with no such superficial vein. Evaluated using a quantitative parameter, this higher responsiveness brings contrast to the visibility of target superficial vein in the image. The quantitative parameters used to reconstruct the single thermal image are $\boldsymbol{\tau}$, dT_{norm}, t_{90-10n}, and TAR, of which the resultant images, in each subject, are shown in Table 4. As defined in Section 2.2.3 and 2.2.4, of the four quantitative parameters, τ has a unit of seconds (s), while the other three are dimensionless. Given the recovery rate is higher over the superficial vein, the τ value is lower and vice-versa for the tissue with no superficial vein. Therefore, to calculate the contrast value (W), a transformed $\boldsymbol{\tau}$ image is used as explained in Section 2.3. A similar image transformation is performed for t_{90-10n} images. Except for Subject-2, the $\boldsymbol{\tau}$ image in other two subjects provide a contrast value of higher than 1 (Table 5), which can be corroborated from the visual inspection of the images (Table 4).

For the case of dT_{norm} and t_{90-10n}, the superficial vein part of the reconstructed images, in all subjects, is found distorted and blurred (Table 4) which is reflected in the lower value of contrast as well (Table 5). In a numerical study, on comparison of parametrization methods applied to ADT on a skin flap model with blood vessel perforator, by Moderhak [24], the contrast value, for the first order $\boldsymbol{\tau}$, dT_{norm}, and t_{90-10n} images, is found to be 0.05, 0.11 and 0.06, respectively. For the $\boldsymbol{\tau}$ and t_{90-10n} images, it should be noted that the contrast is calculated without any image transformation. Using the proposed transformation in the present study (Equation 13), the new value of contrast, for $\boldsymbol{\tau}$ and t_{90-10n} images in [24], is calculated to be 0.06 and 0.08,

respectively. The contrast value for dT_{norm} and t_{90-10n} images in both the studies, numerical [24] and present experimental, is found to be less than 1. Given, the ADT procedure and the skin tissue model used, in the numerical study and the present experimental study, are different, comparison among the same kind of parametric images, between the two studies, is not possible. However, the relative difference in the outcome of the different parametric image reconstruction methods, between the two studies, can be compared. From $\boldsymbol{\tau}$ to dT_{norm} and t_{90-10n}, the numerical study shows an improvement of 33% and 83% in the image contrast value, respectively, while, among the three subjects, the present experimental study shows a minimum and maximum improvement of 50% and 493% from dT_{norm} to $\boldsymbol{\tau}$ and 173% and 786% from t_{90-10n} to $\boldsymbol{\tau}$, respectively (Table 5).

Being one of the parametric methods that depends on the tissue recovery rate, the lower value of contrast in case of dT_{norm} and t_{90-10n} images is possibly because of the inclusion of data until the end of recovery phase as per the definition of these parameters (Equations 6 and 7). It is imperative that as the recovery process approaches towards the end, the temperature difference, between the current skin tissue recovery temperature and the initial temperature (T_i), decreases, which leads to a reduction in the rate of recovery (Figure 2). Hence, the contrast between the tissue with and without vein also decreases, which affects the overall quality of the image; resulting into blurred and distorted images (dT_{norm} and t_{90-10n} images in Table 4). Hence, to satisfy both the conditions, viz. use of rate of recovery as a parameter while considering the data from the initial stages of the recovery process, the TAR parameter is used. This is done by defining a fixed minimax reference recovery temperature value (T_r), within the total recovery phase duration, for all the pixels in the cooling zone. Given the fact that the tissue with

superficial vein will rewarm to T_r temperature with a lower value of t_r, while a higher value of t_r for the same T_r over the tissue with no superficial vein, the resulting TAR value will have a higher contrast between the two regions. Visual inspection of the TAR images (Table 4), in all the subjects, reveals a high qualitative visibility of the superficial vein. As compared to the other image reconstruction methods used in the present study, the TAR images are found to be much better in all subjects. Quantitatively, the contrast value of TAR image, in all the subjects, is found to be more than 1, which signifies a higher visibility of the superficial vein with respect to the background (Table 5).

3.4. Comparative analysis

For each subject, comparing among the image reconstruction methods considered, the value of contrast (W) is found to be highest for TAR method along with a high-quality image, except for TSR coefficient method in Subject-2 and 3 (contrast values do not comply with the respective images). Other than the TAR image method, $\boldsymbol{\tau}$ image is the only method where a contrast value of more than 1 is achieved (except for Subject-2). For the Subject-1, 2, and 3, the improvement in contrast value from $\boldsymbol{\tau}$ image to TAR image is found to be 33%, 243%, and 19%, respectively. For Subject-2, excluding the TSR coefficient method from the analysis, except for TAR image method with a contrast value of 1.03, all other methods give a contrast value in the range of 0.20 to 0.37. Among the non-parametric image reconstruction methods, except for TSR coefficient method, subtracted image provides the highest contrast value. The contrast of the subtracted images, in all the subjects, is found even higher than two of the parametric image reconstruction methods, i.e. dT_{norm} and t_{90-10n}. Unlike for Subject-1 and 3, a similar trend is observed for parametric $\boldsymbol{\tau}$ image in Subject-2.

4. Conclusions

Active dynamic thermography (ADT) is performed on the forearm of three human subjects, using cold thermal stimulation, to produce high contrast image of the superficial vein with the application of single image reconstruction methods. These methods are categorized into non-parametrized and parametrized groups. While for non-parametrized groups, the best image is selected using maximum contrast values, for non-parametrized group, the output image is itself the best contrast image. Further, a qualitative and quantitative comparative study is performed, wherein it is found that the parameterized based TAR image reconstruction method provides the best contrast image, followed by Tau time ($\boldsymbol{\tau}$) image method. In the non-parametrized image reconstruction group, the best method is found to be sequentially subtracted image method. Given the conclusions of the present study is limited to ADT experimentation on three human subjects, subsequent studies on a larger patient cohort shall be performed in future.

Disclosure statement

No potential conflict of interest was reported by the authors.

Funding

The work has been supported by SingHealth-NTU collaborative research grant (Grant number: SHS-NTU/014/2016).

Acknowledgment

The authors would like to acknowledge their heartfelt gratitude to Eetarp Engineering Pte. Ltd., Singapore for providing the IR thermal camera support, and Mr. Gaurav Singh, Ph.D. Scholar,

School of Computer Science and Engineering, NTU Singapore, for his consultation on image processing.

References

[1] Y. V. Gulyaev, A. G. Markov, L. G. Koreneva, and P. V. Zakharov, "Dynamical Infrared Thermography in Humans," *IEEE Eng. Med. Biol. Mag.*, vol. 14, no. 6, pp. 766–771, 1995.

[2] Y. Ohashi and I. Uchida, "Applying dynamic thermography in the diagnosis of breast cancer," *IEEE Eng. Med. Biol. Mag.*, vol. 19, no. 3, pp. 42–51, 2000.

[3] A. Nowakowski, "Quantitative Active Dynamic Thermal IR-Imaging and Thermal Tomography in Medical Diagnostics," in *Medical Devices and Systems*, 3rd ed., J. D. Bronzino, Ed. Taylor & Francis Group, LLC, 2006, pp. 1–30.

[4] H. Dupuis, "Thermographic assessment of skin temperature during a cold provocation test," *Scand. J. Work. Environ. Heal.*, vol. 13, no. 4, pp. 352–355, 1987.

[5] R. B. Barnes, "Barnes : Thermography," *Ann. N. Y. Acad. Sci.*, vol. 121, pp. 34–38, 1964.

[6] N. Bouzida, A. H. Bendada, J.-M. Piau, M. Akhloufi, X. Maldague, and M. Raymond, "Using lock-in infrared thermography for the visualization of the hand vascular tree," in *Proc. of SPIE*, 2008, vol. 6939, pp. 1–12.

[7] D. Wu, H. Hamann, A. Salerno, and G. Busse, "Lockin thermography for imaging of modulated flow in blood vessels," *Conf. Quant. InfraRed Thermogr. Pisa*, pp. 1–5, 1997.

[8] C. Boué, F. Cassagne, C. Massoud, and D. Fournier, "Thermal imaging of a vein of the forearm: Analysis and thermal modelling," *Infrared Phys. Technol.*, vol. 51, no. 1, pp. 13–20, 2007.

[9] W.-M. Liu, J. Meyer, C. G. Scully, E. Elster, and A. M. Gorbach, "Observing temperature

fluctuations in humans using infrared imaging.," *Quant. Infrared Thermogr. J.*, vol. 8, no. 1, pp. 21–36, 2011.

[10] B. Oswald-Tranta, A. Maier, and R. Schledjewski, "Defect depth determination in a CFRP structure using TSR technique," in *Proceedings of the 2014 International Conference on Quantitative InfraRed Thermography*, 2014, pp. 1–8.

[11] F. López, V. P. Nicolau, C. Ibarra-Castanedo, S. Sfarra, and X. Maldague, "Comparative study of thermographic signal reconstruction and partial least squares thermography for the detection and evaluation of subsurface defects Flash-lamps," in *QIRT 2014 Conference*, 2014, no. 1, pp. 1–10.

[12] J. Roche, F. Leroy, and D. L. Balageas, "Information condensation in defect detection using TSR coefficients images," in *QIRT2014 Conférence*, 2014, no. 1, pp. 1–10.

[13] D. L. Balageas, J. M. Roche, F. H. Leroy, W. M. Liu, and A. M. Gorbach, "The thermographic signal reconstruction method: A powerful tool for the enhancement of transient thermographic images," *Biocybern. Biomed. Eng.*, vol. 35, no. 1, pp. 1–9, 2015.

[14] Liu, Wei-Min, Jordan Maivelett, Gregory J. Kato, James G. Taylor, Wen-Chin Yang, Yun-Chung Liu, You-Gang Yang, and Alexander M. Gorbach, "Reconstruction of thermographic signals to map perforator vessels in humans," *Quant. Infrared Thermogr. J.*, vol. 9, no. 2, pp. 123–133, 2012.

[15] Foerster, J., S. Wittstock, S. Fleischanderl, A. Storch, G. Riemekasten, O. Hochmuth, B. Meffert, H. Meffert, and M. Worm, "Infrared-monitored cold response in the assessment of Raynaud's phenomenon," *Clin. Exp. Dermatol.*, vol. 31, no. 1, pp. 6–12, 2005.

[16] M. Kaczmarek, A. Nowakowski, M. Suchowirski, J. Siebert, and W. Stojek, "Active

dynamic thermography in cardiosurgery," *Quant. Infrared Thermogr. J.*, vol. 4, no. 1, pp. 107–123, 2007.

[17] Nowakowski A, Kaczmarek M, Stojek W, Beta S, Trzeciak B, Topolewicz J, Rogowski J, Siebert J, "IR-thermal monitoring of cardiosurgery interventions," in *IFMBE Proceedings 22*, 2008, pp. 1329–1333.

[18] A. Nowakowski, P. Siondalski, M. Moderhak, and M. Kaczmarek, "A new diagnostic method for evaluation of cardiosurgery wound healing," *Quant. Infrared Thermogr. J.*, vol. 13, no. 1, pp. 19–34, 2016.

[19] A. Renkielska *et al.*, "Active dynamic infrared thermal imaging in burn depth evaluation," *J. Burn Care Res.*, vol. 35, no. 5, pp. e294–e303, 2014.

[20] A. Renkielska, A. Nowakowski, M. Kaczmarek, and J. Ruminski, "Burn depths evaluation based on active dynamic IR thermal imaging-A preliminary study," *Burns*, vol. 32, no. 7, pp. 867–875, 2006.

[21] J. Rumiński, M. Kaczmarek, A. Renkielska, and A. Nowakowski, "Thermal parametric imaging in the evaluation of skin burn depth," *IEEE Trans. Biomed. Eng.*, vol. 54, no. 2, pp. 303–312, 2007.

[22] S. Jankovic, S. Stankovic, S. Borjanovic, L. Tenjovic, and M. Bogdanovic, "Cold stress dynamic thermography for evaluation of vascular disorders in hand-arm vibration syndrome," *J Occup Heal.*, vol. 50, no. 5, pp. 423–425, 2008.

[23] M. Moderhak, S. Kołacz, J. Jankau, and T. Juchniewicz, "Active dynamic thermography method for TRAM flap blood perfusion mapping in breast reconstruction," *Quant. Infrared Thermogr. J.*, vol. 14, no. 2, pp. 234–249, 2017.

[24] M. Moderhak, “Comparison of the exponential thermal transient parameterization methods with the SMTP method in the unipedicled DIEP flap computer modelling and simulation,” *Quant. Infrared Thermogr. J.*, vol. 6733, pp. 1–12, 2018.

[25] A. Saxena, V. Raman, and E. Y. K. Ng, “Single image reconstruction in active dynamic thermography: A novel approach,” *Infrared Phys. Technol.*, vol. 93, no. Sept., pp. 53–58, 2018.

[26] A. Saxena, E. Y. K. Ng, and V. Raman, “Thermographic venous blood flow characterization with external cooling stimulation,” *Infrared Phys. Technol.*, vol. 90, pp. 8–19, 2018.

[27] C. Ibarra-Castanedo and X. Maldague, “Pulsed phase thermography reviewed,” *Quant. Infrared Thermogr. J.*, vol. 1, no. 1, pp. 47–70, 2004.

[28] R. W. Lewis, P. Nithiarasu, and K. N. Seetharamu, *Fundamentals of the Finite Element Method for Heat and Fluid Flow*, vol. 3. John Wiley & Sons, Ltd, 2004.

[29] G. R. North, “Lessons from energy balance models,” in *Physically-Based Modelling and Simulation of Climate and Climatic Change-Part II*, vol. 1, M. E. Schlesinger, Ed. Kluwer Academic Publishers, 1988, pp. 627–651.

[30] H. Meffert, N. Sonnichsen, and B. Meffert, “Skin-rewarming curves,” *Lancet*, vol. 7780, pp. 769–770, 1972.

[31] A. Merla, L. Di Donato, S. Di Luzio, and G. L. Romani, “Quantifying the relevance and stage of disease with the tau image technique,” *IEEE Eng. Med. Biol. Mag.*, vol. 21, no. 6, pp. 86–91, 2002.

[32] E. Peli, “Contrast in complex images,” *J. Opt. Soc. Am. A*, vol. 7, no. 10, p. 2032, 1990.

Figure 1: Experimental setup: 1) Infrared thermal camera 2) Tripod to fix the camera 3) Human subject forearm 4) Cooling pad to apply the external stimulation

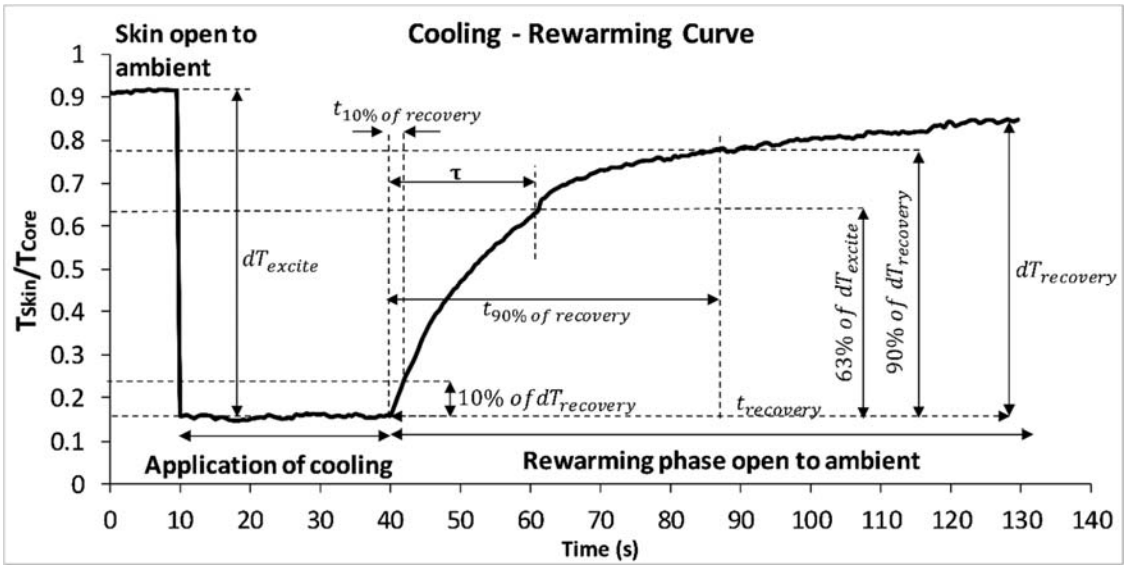

Figure 2: Cooling-rewarming curve in active dynamic thermography depicting curve variables (T_{Core}=37 ^oC)

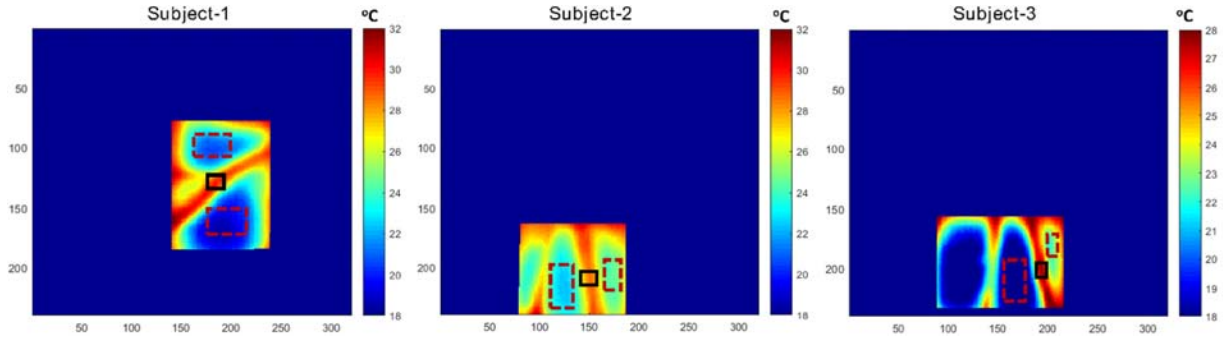

Figure 3: Reference location I and I_b selection in the image: black box is over the blood vessel (I) and red-dashed box is outside the vessel (I_b)

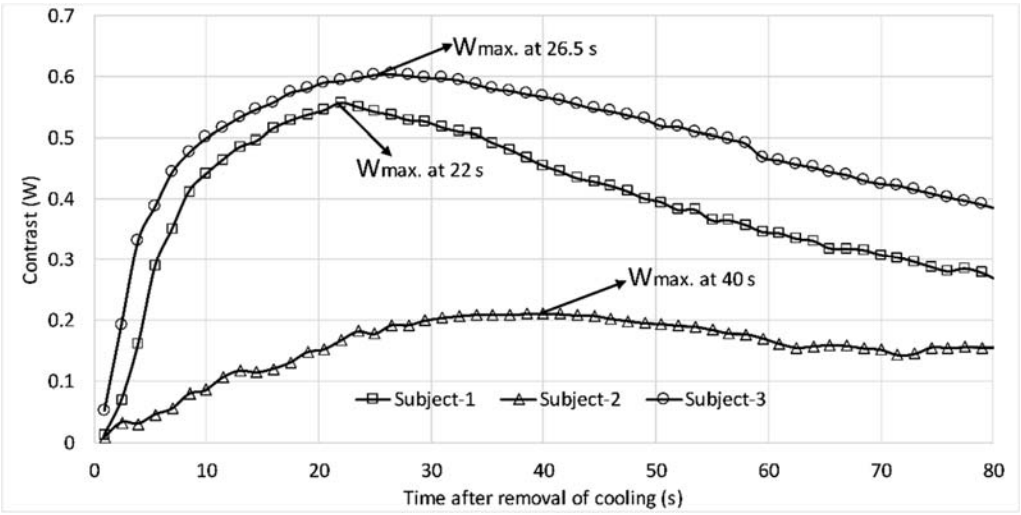

Figure 4: Contrast versus time after removal of cooling for the original sequence of thermal images

Table 1: External cooling stimulation details

Subject Studied	Average temperature within the cooling stimulation zone (°C) ± SD		
	Before cooling (t=5s)	**After cooling (t=40s)**	**End of rewarming (t=130s)**
Subject-1	33.53 ± 0.12	8.53 ± 3.5	27.27 ± 1.87
Subject-2	33.52 ± 0.19	9.53 ± 1.98	28.55 ± 1.68
Subject-3	32.82 ± 0.33	9.42 ± 1.03	25.09 ± 2.90

Table 2: Best contrast image in ADT sequence

	Subject-1	Subject-2	Subject-3
Sequence (at $W_{max.}$)	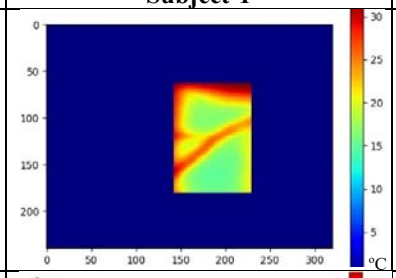	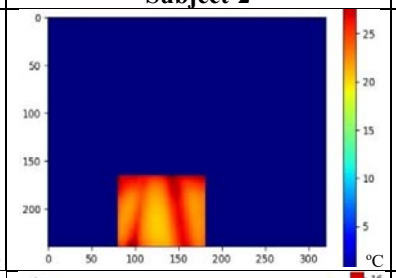	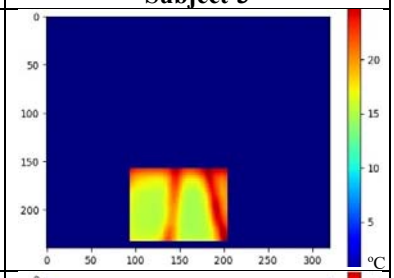
Subtracted (at $W_{max.}$)	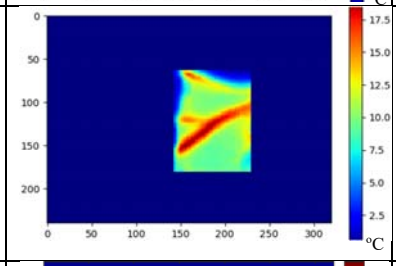	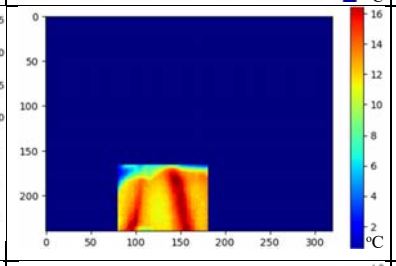	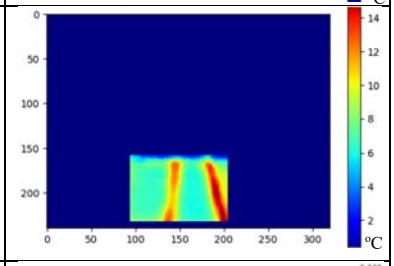
Amplitude	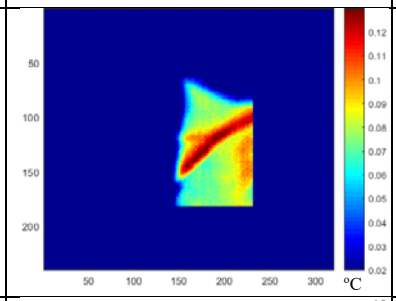	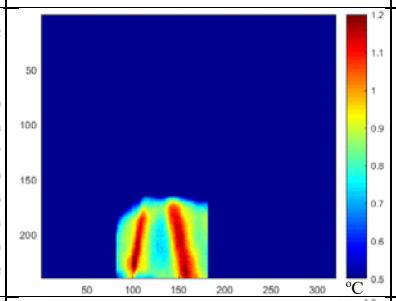	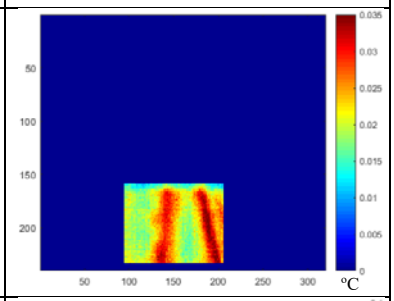
Phase	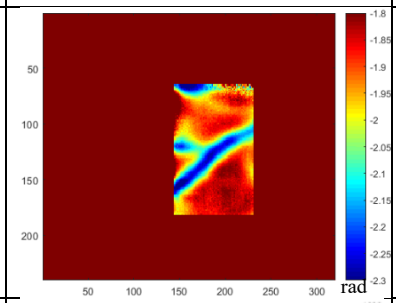	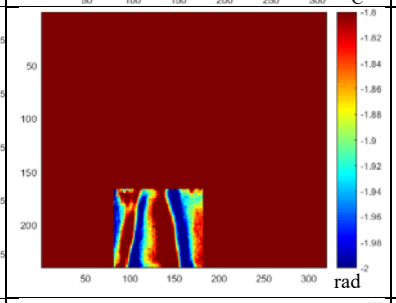	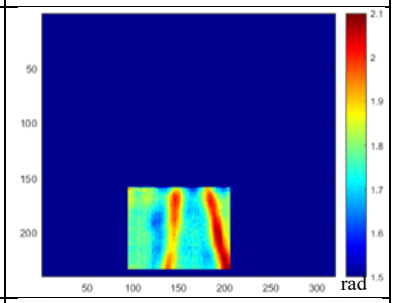
TSR	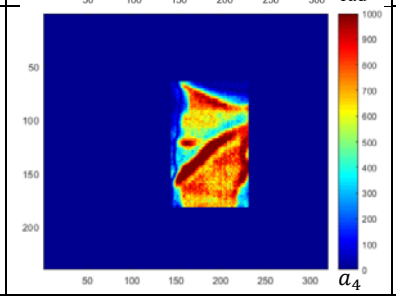	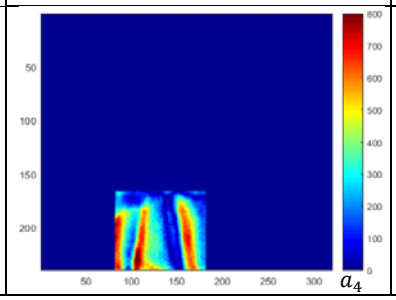	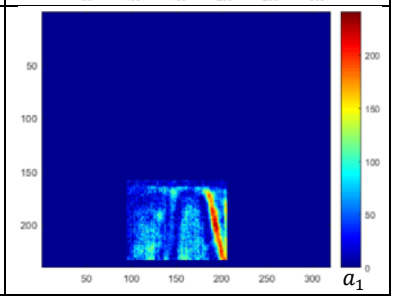

Table 3: Contrast (W) value of first derivative TSR coefficient images at $m = 4, 5, and\ 6$

Coefficient Image	Image Contrast (W) in TSR images								
	Subject 1			Subject 2			Subject 3		
	$m = 4$	$m = 5$	$m = 6$	$m = 4$	$m = 5$	$m = 6$	$m = 4$	$m = 5$	$m = 6$
a_1	0.817	0.079	0.061	1.734	1.613	0.088	1.140	1.904	1.036
a_2	0.830	0.091	0.061	1.920	1.558	0.433	1.146	1.885	1.042
a_3	0.842	0.105	0.062	2.240	1.498	1.899	1.152	1.866	1.048
a_4	0.852	0.119	0.063	2.844	1.432	0.165	1.158	1.848	1.053
a_5	NA	0.135	0.064	NA	1.358	0.751	NA	1.830	1.059
a_6	NA	NA	0.066	NA	NA	0.519	NA	NA	1.065

Table 4: Image output from different single image reconstruction methods in ADT

	Subject-1	Subject-2	Subject-3
τ	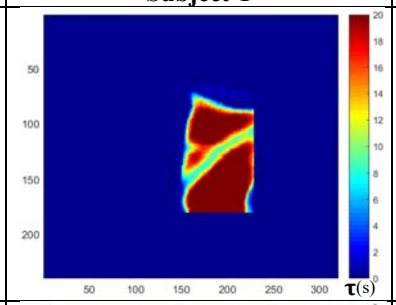	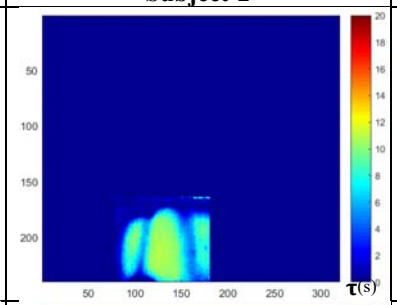	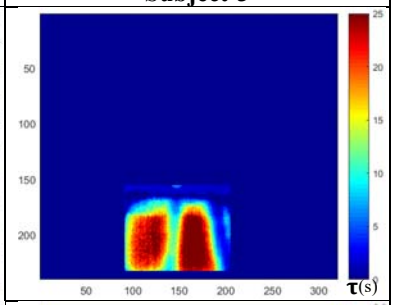
dT_{norm}	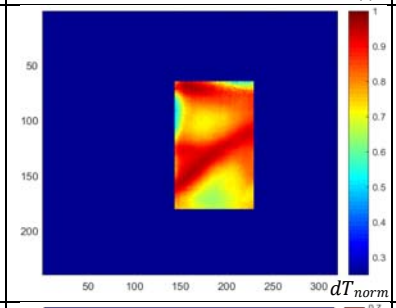	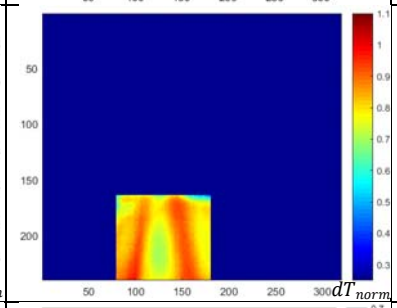	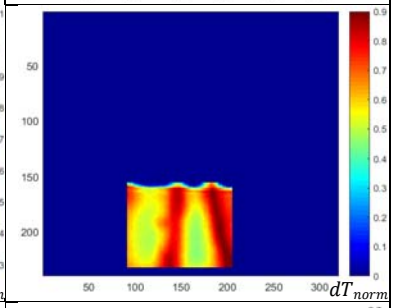
t_{90-10n}	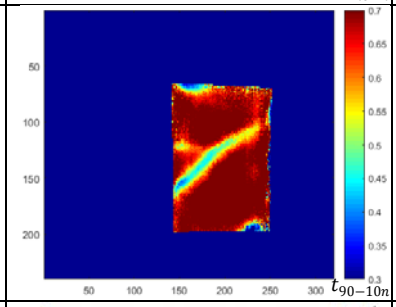	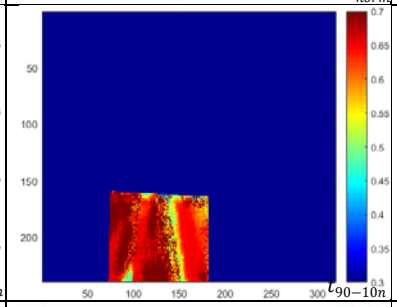	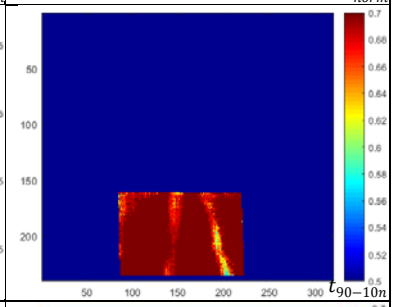
TAR	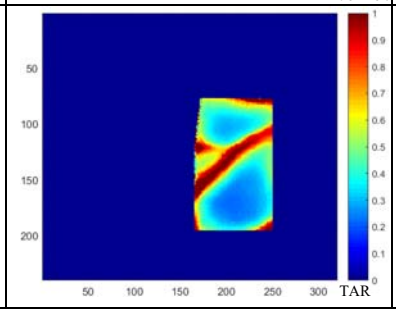	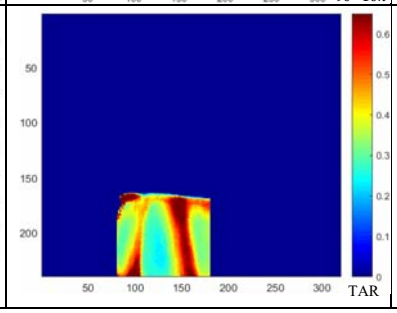	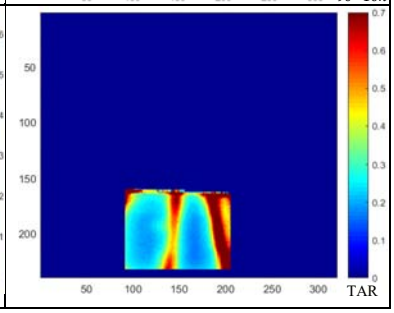

Table 5: Contrast and image parameter value over the skin tissue with (target, I) and without (background, I_b) the superficial vein in the reconstructed image from different image reconstruction methods

Image Reconstruction Methods		**Contrast (W)**		
		Subject 1	**Subject 2**	**Subject 3**
Sequence Image (W_{max})		0.56 I=23.87 °C, I_b=15.30 °C	0.21 I=26.34 °C, I_b=21.79 °C	0.61 I=23.83 °C, I_b=14.80 °C
Subtracted Image (at sequence W_{max})		0.85 I=18.14 °C, I_b=9.80 °C	0.37 I=16.36 °C, I_b=11.96 °C	0.78 I=11.58 °C, I_b=6.50 °C
Fourier Transform	Amplitude	0.53 I=0.12 °C, I_b=0.07 °C	0.35 I=1.11 °C, I_b=0.82 °C	0.50 I=0.03 °C, I_b=0.02 °C
	Phase	0.20* I'=1.46, I_b'=1.22	0.04* I'=1.22, I_b'=1.17	0.18 I=2.04 rad, I_b=1.72 rad
Thermographic Signal Reconstruction (TSR)		0.85 I=1230, I_b=664	2.84 I=615, I_b=160	1.90 I=205, I_b=70.70
Parametric Image Reconstruction	$\boldsymbol{\tau}$	1.78* I'=3.99, I_b'=1.43	0.30* I'=1.87, I_b'=1.44	1.24* I'=3.09, I_b'=1.38
	dT_{norm}	0.30 I=0.94, I_b=0.73	0.20 I=0.91, I_b=0.76	0.54 I=0.81, I_b=0.53
	t_{90-10n}	0.60* $I' = 1.93$, I_b'=1.21	0.11* I'=1.41, I_b'=1.28	0.14* I'=1.26, I_b'=1.10
	Tissue Activity Ratio (TAR)	2.37 I=1.01, I_b=0.30	1.03 I=0.61, I_b=0.30	1.47 I=0.52, I_b=0.21

I: Image parameter over the skin tissue with superficial vein (target)
I_b: Image parameter over the skin tissue without superficial vein (background)
*Contrast (W) is calculated after the transformation of the images (I' and I_b' of I and I_b, respectively) using Equation 13 (I' and I_b' are dimensionless)